A large displacement, high frequency, underwater microelectromechanical systems actuator

David J. Hoelzle,[1,a)] Clara K. Chan,[2,3] Michael B. Scott,[2,4] Melinda A. Lake,[1] and Amy C. Rowat[2,3,5,b)]

[1]*Department of Aerospace and Mechanical Engineering, University of Notre Dame, Notre Dame, Indiana 46556, USA*
[2]*Department of Integrative Biology and Physiology, University of California, Los Angeles, Los Angeles, California 90095, USA*
[3]*Department of Bioengineering, University of California, Los Angeles, Los Angeles, California 90095, USA*
[4]*Department of Mechanical and Aerospace Engineering, University of California, Los Angeles, Los Angeles, California 90095, USA*
[5]*Center for Biological Physics, Jonsson Comprehensive Cancer Center, and Broad Stem Cell Center, University of California, Los Angeles, Los Angeles, California 90095, USA*

(Received 15 June 2014; accepted 18 December 2014; published online 6 January 2015)

Here, we demonstrate an *in situ* electrostatic actuator that can operate underwater across a wide range of displacements and frequencies, achieving a displacement of approximately 10 μm at 500 Hz and 1 μm at 5 kHz; this performance surpasses that of existing underwater physical actuators. To attain these large displacements at such high speeds, we optimized critical design parameters using a computationally efficient description of the physics of low quality (Q) factor underwater electrostatic actuators. Our theoretical model accurately predicts actuator motion profiles as well as limits of bandwidth and displacement. © *2015 AIP Publishing LLC*. [http://dx.doi.org/10.1063/1.4905385]

I. INTRODUCTION

The pinnacle of a microfluidic very large systems integration (VLSI) system is a network of thousands of densely packed transducers that each perform a dedicated function within micron-scale channels.[1] To manipulate conveyed particles or fluid streams, physical actuators are an important type of functional transducer that has transformed biological and chemical assays.[2] For example, dense arrays of polydimethylsiloxane (PDMS) valves are integrated into microfluidic channels to coordinate 10^2–10^3 distinct protein interactions in parallel.[1] These diaphragm valves can achieve $O(10^{-5})$ m displacements at frequencies up to 100 Hz.[3] Similar PDMS diaphragm actuators can be integrated into the side of a microfluidic channel to perturb flows for particle sorting; these can achieve smaller $O(10^{-6})$ m displacements at 250 Hz.[4] While these PDMS actuators have significantly advanced the functionality of microfluidic VLSI networks, a physical actuator that could operate across an even larger range of frequencies and displacements would enable new, potentially transformative functions. For instance, an actuator with a displacement range of $O(10^{-5})$ m and 1 kHz bandwidth could enable in-channel optical modulation or even high throughput deformation of cells within a microfluidic channel. At higher frequencies of 10 kHz and with a displacement of $O(10^{-6})$ m, an *in situ* physical actuator could generate local acoustic waves to entrain biological species in micron-scale vortices.[5] Given these potentially transformative applications, we aim to design a compact, underwater actuator that can attain a displacement of $O(10^{-5})$ m at frequencies in the range of 100 Hz–1 kHz and a displacement of $O(10^{-6})$ m at frequencies of $O(10^4)$ Hz.

A silicon-based physical actuator has the potential to attain up to 10^{-5} m displacements at 1 kHz (Fig. 1).[7] The natural frequency of an actuator is $\omega_n = \sqrt{k/m}$, where k is the spring constant and m is the mass; therefore, the modulus to density ratio of the material composing the actuator provides a measure of its achievable bandwidth. Silicon has a modulus to density ratio that is over four orders of magnitude

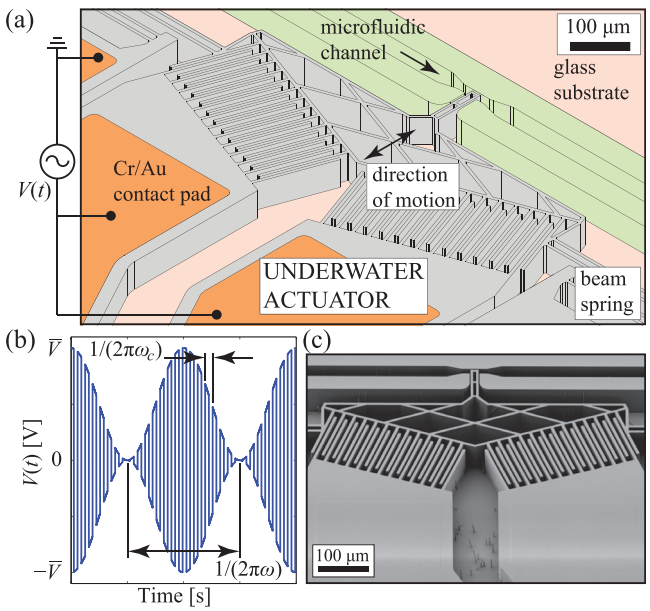

FIG. 1. (a) Electrostatic physical actuator. Perforated members are suspended and monolithic members are bonded to glass. (b) Amplitude modulated voltage signal for underwater actuation. (c) Scanning electron micrograph of the actuator fabricated by micromachining low-resistivity silicon bonded to glass.[6]

a)Electronic mail: dhoelzle@nd.edu
b)Electronic mail: rowat@ucla.edu

larger than PDMS: an actuator fabricated from silicon can thus achieve a bandwidth that is over two orders of magnitude larger than a PDMS actuator. Moreover, there are well-developed tools to micromachine silicon wafers into complex geometries with compact form factors; in contrast, piezoelectric actuators are too large to be integrated into micron-scale channels at high unit density.[8]

To attain the stringent performance objectives required for advanced microfluidic VLSI units, we must first understand the physics of actuators immersed in aqueous media. The fluid surrounding the actuator is the strongest determinant of the quality (Q) factor.[9,10] Actuators in air or vacuum have high Q-factors, while those immersed in water typically have Q-factors that are at least four orders of magnitude smaller. The motion profiles of high Q-factor actuators are described by perturbation methods,[11] which assume that $|Q^{-1}| \ll 1$; this assumption is not valid for low-Q physics. Here, we develop the theory to describe actuator motion in the low-Q range of $Q \sim O(10^{-5}$–$10^{0})$; experimental results have a strong agreement with this theoretical model.

II. NONLINEAR MODEL AND OPTIMIZATION

A sprung mass with a single degree-of-freedom in a viscous medium is simply modeled as a mass-spring-damper system (Fig. 2(a)) with the equation of motion

$$m\ddot{x}(t) + b\dot{x}(t) + kx(t) = F(x, V). \tag{1}$$

Here, m is the actuator mass assumed as a point-mass, b is the damping coefficient, k is the spring constant, $x(t)$ is the generalized coordinate, and $F(x, V)$ is an electrostatic force in the direction of the generalized coordinate.

Two deleterious phenomena preclude the utility of actuators immersed in water:[12] (1) Electrolysis at the charged surfaces occurs at potential differences above 8 V and thus constrains the applied voltage to $V(t) \in [-8, 8]$ V in deionized water; and (2) Water molecules between charged surfaces orient themselves with the electric field, thereby shielding electrostatic forces. Charge shielding can be minimized by using a voltage signal that flips the electrode polarity faster than water molecules physically reorient.[12] A desired electrostatic force can thus be generated by applying an amplitude modulated voltage signal (Fig. 1(b)) in which a desired fundamental signal has frequency content on the order of the actuator bandwidth and a high-frequency carrier wave flips polarity every $\frac{1}{4\pi\omega_c}$ s; ω_c should be approximately two orders of magnitude larger than the bandwidth.

The electrostatic force of an actuator with an applied amplitude modulated voltage is given by Eq. (2), where the position and voltage dependent components are separable

$$\begin{aligned} F(x,V) &= f(x)V^2(t), \\ F(x,V) &= f(x)\left(\frac{1}{2}\bar{V}(1+\cos\omega t)\Pi(t)\right)^2 \\ &= f(x)\bar{V}^2\left(\frac{3}{8}+\frac{1}{2}\cos\omega t+\frac{1}{8}\cos 2\omega t + H.F.T.\right), \end{aligned} \tag{2}$$

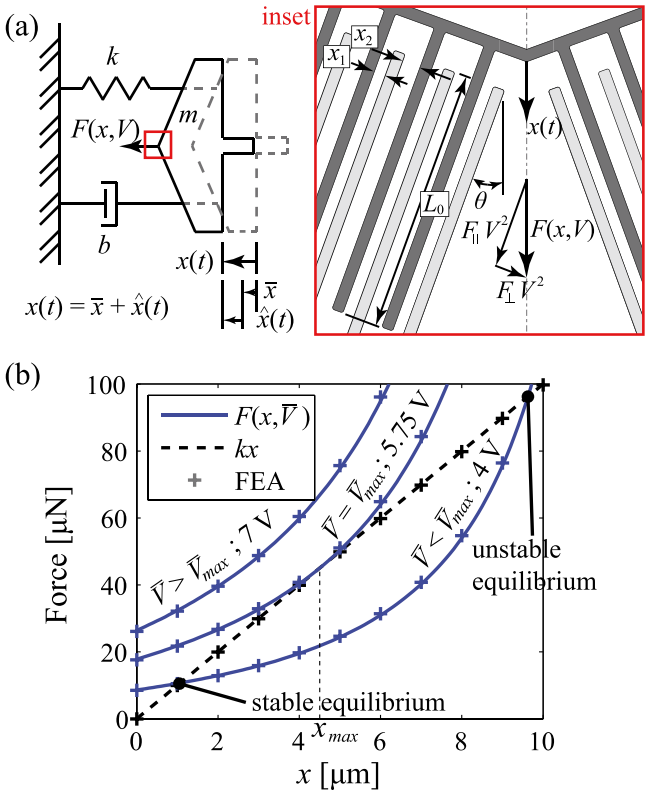

FIG. 2. (a) Model of an electrostatic actuator in an aqueous medium. The inset shows the resultant force $F(x, V)$ from the parallel $F_{\parallel}$ and perpendicular $F_{\perp}$ force components acting on the comb fingers. The moving comb is dark gray and the stationary comb is light gray. The force perpendicular to $F(x, V)$ is theoretically equal to zero as the drive is symmetric about the centerline, which is denoted by the dashed line. (b) Static forces for an actuator with $k = 10\,\mathrm{N\,m^{-1}}$ and $\theta = 20°$. The equilibrium position $x(t)$ given a constant applied voltage has two solutions for $\bar{V} < \bar{V}_{max}$ and one solution, x_{max}, for $\bar{V} = \bar{V}_{max}$. Finite Element Analysis (FEA) force calculations are based on the geometry of the model in Fig. 1(a).

and $\Pi(t) = \frac{4}{\pi}\sum_{j=1}^{\infty}\frac{1}{2j-1}(-1)^{j-1}\cos\omega_c jt$ is the Fourier series of a pulse-type carrier wave. After simplification, $\Pi^2(t)$ has a unit magnitude DC term plus an infinite sum of high frequency terms (*H.F.T.*) that are inconsequential to actuator position.

The two most common electrostatic comb drive orientations are transverse drives ($\theta = 90°$), which exert large forces but are limited to small displacements, and longitudinal drives ($\theta = 0°$), which achieve large displacements but exert small forces (Fig. 2(a)). In contrast, a hybrid drive ($\theta \in (0°, 90°)$) of comparable size can exert a force that is approximately three times greater than a longitudinal drive and achieve a displacement that is approximately three times larger than a transverse drive. Such a hybrid actuator design is thus advantageous for microfluidic VLSI as the footprint can be reduced without sacrificing functionality. The position dependent component of a hybrid drive is given by

$$\begin{aligned} f(x) &= F_{\parallel}\cos\theta + F_{\perp}\sin\theta, \\ F_{\parallel} &= \frac{1}{2}\left(\frac{1}{x_1 - x\sin\theta}+\frac{1}{x_2 + x\sin\theta}\right)\kappa\epsilon hM, \\ F_{\perp} &= \frac{1}{2}\frac{(L_0 + x\cos\theta)(x_1+x_2)(x_2 - x_1 + 2x\sin\theta)}{(x_1 - x\sin\theta)^2(x_2 + x\sin\theta)^2}\kappa\epsilon hM, \end{aligned} \tag{3}$$

TABLE I. Geometric and physical parameters.

$m = 1.34 \times 10^{-9}$ kg	$x_1 = 5\ \mu$m	$h = 45\ \mu$m
$b = 1.25 \times 10^{-3}$ N s m^{-1}	$x_2 = 8\ \mu$m	$M = 26$ pairs
$k \in (0, 15]$ N m^{-1}	$L_0 = 115\ \mu$m	$\theta \in (0°, 90°)$
κ (in water) $= 78$	$\epsilon = 8.854 \times 10^{-12}$ s^{4}A^{2}m^{-3}kg^{-1}	

where $F_{\parallel}$ and $F_{\perp}$ are the components parallel[12] and perpendicular[13] to the face of the combs. Geometric parameters θ, L_0, x_1, and x_2 are shown in Fig. 2(a). The other geometric parameters are the comb height, h, and the number of comb pairs, M. The two physical parameters are κ, the dielectric constant of the immersing medium (1 for air, 78 for deionized water), and ϵ, the permittivity of free space (Table I).

Static actuator displacement as a function of applied voltage is calculated by solving the nonlinear equation $kx = F(x, V)$ at $V(t) = \bar{V}$. For $\bar{V} < \bar{V}_{max}$, there is always one stable and one unstable solution (Fig. 2(b)). As $\bar{V}$ is increased to $\bar{V}_{max}$, the stable and unstable solutions converge to a double-root x_{max}, which is the maximum stable displacement of the actuator. There is no solution for $\bar{V} > \bar{V}_{max}$, yielding the well-known "pull-in" instability.[14] Finite Element Analysis complements Eqs. (2) and (3), with less than a 5% error across the range of relevant voltages and displacements (Fig. 2(b)).

The dynamics of the actuator are collectively described by Eqs. (1)–(3). The DC term of Eq. (2), $\frac{3}{8}f(x)\bar{V}^2$, imparts a DC offset in the position, $\bar{x}$, that is solved by numerical methods. x is rewritten as a deviation from the DC offset position, $x(t) = \bar{x} + \hat{x}(t)$, and Eqs. (1)–(3) are expanded as a Taylor series to the third-order, evaluated at $\bar{x}$, Eq. (4a)

$$m\ddot{\hat{x}} + b\dot{\hat{x}} + k(\hat{x} + \bar{x}) = \left(f(\bar{x}) + \frac{\partial f(\bar{x})}{\partial x}\hat{x} + \frac{1}{2}\frac{\partial^2 f(\bar{x})}{\partial x^2}\hat{x}^2 + \frac{1}{6}\frac{\partial^3 f(\bar{x})}{\partial x^3}\hat{x}^3\right)V^2, \tag{4a}$$

$$\ddot{\hat{x}} + Q^{-1}\dot{\hat{x}} + (a_{10} + a_{11}\cos\tau + a_{12}\cos 2\tau)\hat{x} + (a_{20} + a_{21}\cos\tau + a_{22}\cos 2\tau)\hat{x}^2 + (a_{30} + a_{31}\cos\tau + a_{32}\cos 2\tau)\hat{x}^3 = a_{01}\cos\tau + a_{02}\cos 2\tau, \tag{4b}$$

$$T(\tau)\mathbf{\Delta}^2 X + Q^{-1}T(\tau)\mathbf{\Delta}X + T(\tau)(a_{10} + a_{11}\mathbf{C}_1 + a_{12}\mathbf{C}_2)X + T(\tau)(a_{20} + a_{21}\mathbf{C}_1 + a_{22}\mathbf{C}_2)\mathbf{\Gamma}(X)X + T(\tau)(a_{30} + a_{31}\mathbf{C}_1 + a_{32}\mathbf{C}_2)\mathbf{\Gamma}^2(X)X - T(\tau)G = 0. \tag{4c}$$

Equation (4a) is simplified by normalizing time by the fundamental frequency, $\tau = \omega t$, yielding the nonlinear, parameter-varying, non-homogeneous, ordinary differential equation (4b). As the coefficients of the nonlinear terms are less than 0 (Fig. 3(b)), the electrostatic force acts as a weakening spring: thus as deflection increases, the force returning the actuator to the neutral position decreases and yields the "pull-in" instability above a critical x_{max}.

The standard solution to Eq. (4b) utilizes perturbation methods.[11] This is a reasonable solution as the assumption that $|Q^{-1}| \ll 1$ is valid for actuators operated in air or vacuum, which have $Q^{-1} \sim O(10^{-4}$–$10^{-5})$.[14] However, in an underwater environment Q^{-1} is 4–10 orders of magnitude larger; the $|Q^{-1}| \ll 1$ assumption is, thus, invalid. Numerical methods can be used to solve Eq. (4b), however, many coefficient permutations tested in a design optimization algorithm (Fig. 3(b)) will yield systems that are characterized as "stiff," as they have distinct dynamic modes that evolve on drastically different time scales. Implicit and explicit numerical methods are inefficient for "stiff" systems; for example, Eq. (4b) requires 5 h to solve for many coefficient permutations. Clearly, to optimize over a wide range of the actuator design space we need a mathematical description that is computationally efficient, valid for low-Q physics, and universally applicable to a wide parameter range.

The differential equation (4b) is a specific form of the Duffing equation[11] that is both parametrically driven and exogenously driven by harmonic functions. Within the stable displacement limit, the solution to Eq. (4b) is assumed to be an N^{th} order harmonic function with unknown coefficients[17–19]

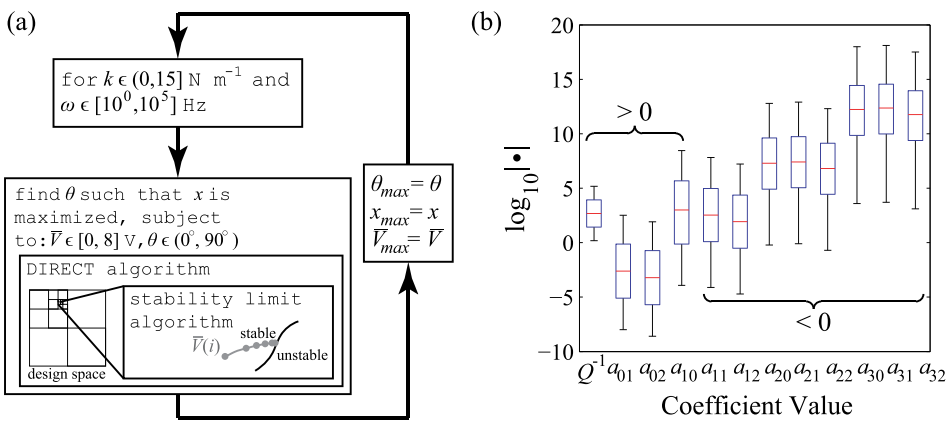

FIG. 3. (a) Algorithm to optimize parameters k and θ. The optimization loop uses the gradient-free DIRECT algorithm[15,16] to find an optimal θ for each k and ω; a gradient-free method must be used because a gradient does not exist at the instability bound corresponding to $x(\tau) = x_{max}$. (b) Coefficient value ranges for Eq. (4b) for all 7007 candidate designs simulated.

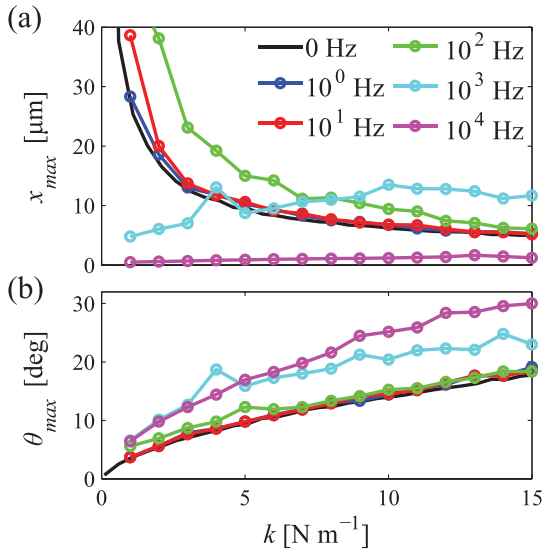

FIG. 4. Optimized design parameter θ for an actuator with a given k and operated at a varying fundamental frequency, ω. (a) Achievable x_{max}. (b) Optimal comb drive angle θ_{max}.

$$x(\tau) = A_0 + A_1 \cos\tau + B_1 \sin\tau + \cdots + A_N \cos N\tau + B_N \sin N\tau. \quad (5)$$

Equation (5) is equivalently stated as $x(\tau) = T(\tau)X$

$$T(\tau) = [1, \cos\tau, \sin\tau, \ldots, \cos N\tau, \sin N\tau],$$
$$X = [A_0, A_1, B_1, \ldots, A_N, B_N]^T, \quad (6)$$

where $T(\tau) \in \mathbb{R}^{1\times 2N+1}$ is an orthogonal harmonic basis vector and $X \in \mathbb{R}^{2N+1\times 1}$ is a vector of unknown coefficients. The orthogonal basis is leveraged to rewrite Eq. (4b) as matrix algebra, Eq. (4c), where $\mathbf{\Delta}$ is the constant matrix that performs the operation $\frac{d}{d\tau}$, $\mathbf{C}_1$, and $\mathbf{C}_2$ are constant matrices that multiply $T(\tau)X$, respectively, by $\cos\tau$ and $\cos 2\tau$, $\mathbf{\Gamma}(X)$ is a matrix of unknown coefficients that perform the operation $x^2(\tau) \approx T(\tau)\mathbf{\Gamma}(X)X$, and $G = [0,\ a_{01},\ 0,\ a_{02},\ 0,\ 0,\ldots]^T$. Explicit constructions of $\mathbf{\Delta}$, $\mathbf{C}_1$, $\mathbf{C}_2$, and $\mathbf{\Gamma}(X)$ are given in the Appendix. Equation (4c) is simplified to the nonlinear matrix equation[19]

$$\mathbf{L}X + P(X) - G = 0.$$

The solution vector X is solved by the Newton-Raphson method

$$X_{n+1} = X_n - \left(\mathbf{L} + \frac{\partial P(X_n)}{\partial X}\right)^{-1} (\mathbf{L}X_n + P(X_n) - G), \quad (7)$$

where n is the iteration index of the algorithm.

Given a stable operating voltage, algorithm (7) converges to a solution vector X in less than ten iterations with an average computation time of 31.6 s on a multi-core desktop computer. The Fourier series solution is two orders of magnitude more efficient than implicit and explicit solvers.

III. OPTIMIZATION RESULTS

We use the DIRECT algorithm[20] to optimize the two design variables that have the largest influence on displacement and bandwidth, k and θ, by evaluating 7007 distinct designs (Fig. 3). The solution vector X_{n+1} in algorithm (7) is called over 130 000 times. Design optimization predicts that the design objectives (displacement of 10^{-5} m at 100 Hz–1 kHz and displacement of 10^{-6} m at 10 kHz) are attainable for an actuator design with $k \in (5, 10)$ N m^{-1} and $\theta \in (10°, 20°)$ (Fig. 4).

Our simulation results show that an underwater actuator with $k = 10$ N m^{-1} and $\theta = 20°$ behaves as a second-order over-damped system (Fig. 5(c)): for a set $\bar{V} = 5.88$ V, the magnitude of $x_{max}(\omega)$ remains constant until approximately 100 Hz, whereafter $x_{max}(\omega)$ decreases with increasing frequency (Figs. 5(a) and 5(c)). At frequencies above 100 Hz, the position $x(t)$ shifts out of phase with the parametrically and exogenously driven terms in Eq. (4b); consequently, a higher displacement can be achieved without introducing "pull-in" instabilities (Figs. 5(b) and 5(c)). This essential knowledge of the frequency dependence of the stable regime is only understood with a nonlinear model of the physics of low-Q actuators.

IV. METHODS

To validate our model, we micromachined an electrostatic actuator with $k = 10$ N m^{-1} and $\theta = 20°$ (Fig. 1(c)) using standard lithographic processes[6] for silicon-on-glass wafers. We then immersed the actuator in deionized water and applied the voltage function in Eq. (2) at different

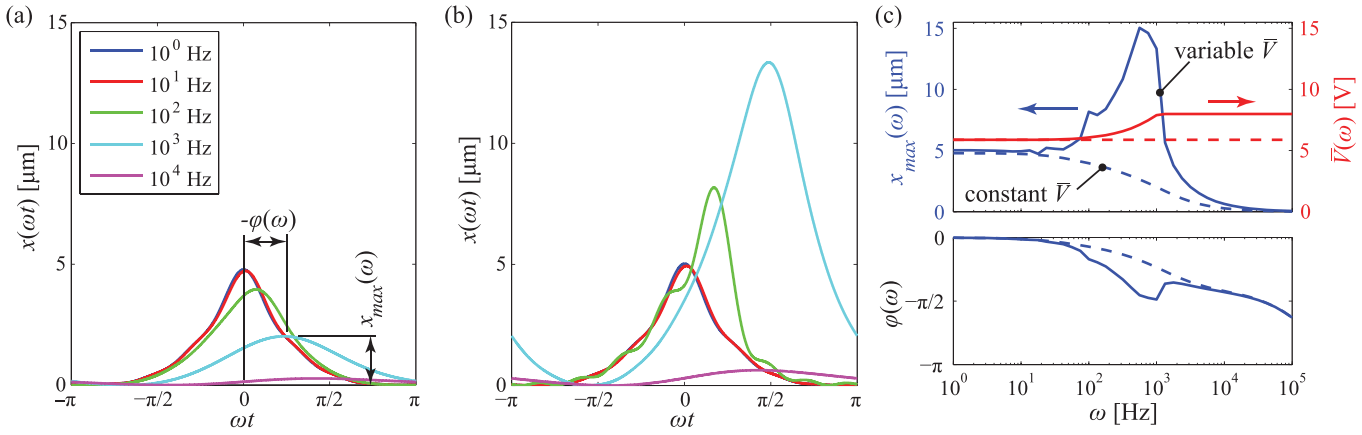

FIG. 5. Simulated time and frequency response for an underwater actuator with $k = 10$ N m^{-1} and $\theta = 20°$. (a) x as a function of normalized time for a constant $\bar{V}$ at select frequencies. (b) x as a function of normalized time at select frequencies operated at a $\bar{V}_{max}$ that maximizes actuator displacement. (c) Simulated frequency response at a constant $\bar{V} = 5.88$ V and at a variable $\bar{V}(\omega)$.

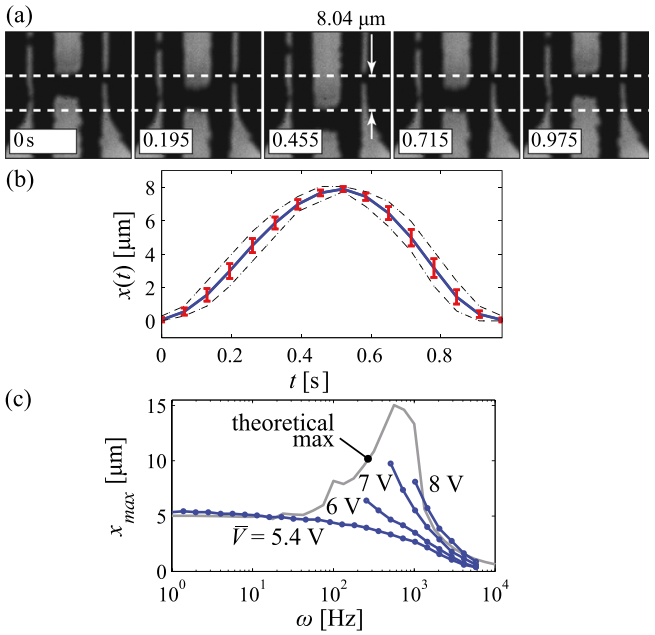

FIG. 6. Large displacement, high frequency underwater actuation. (a) Region-of-interest of the actuator probe for one cycle at a 1024 Hz actuation frequency with $\bar{V} = 8$ V. (b) Position trace for 2000 cycles at 1024 Hz with $\bar{V} = 8$ V. The mean plus and minus one standard deviation is denoted by the error bars and the trace envelope is denoted by the dashed line. (c) Frequency responses at varying $\bar{V}$ levels. Each data point is the mean of at least 80 cycles.

fundamental frequencies ($\omega = 2^0, 2^{0.5}, \ldots, 2^{12}$ Hz) and voltage magnitudes ($\bar{V} = 5.4, 5.5, 6, \ldots, 8$ V) and at a set $\omega_c = 500$ kHz. Displacement profiles were measured by imaging actuator movement with an inverted microscope and a high-speed camera and then processing images with a custom MATLAB script.

V. RESULTS AND DISCUSSION

The experimental frequency response confirms the prediction that the system will be over-damped and hence $Q \ll 1$ (Fig. 6(c)). We observe that an underwater actuator with $k = 10\,\text{N m}^{-1}$ and $\theta = 20°$ can achieve a displacement range of 8 μm at frequencies greater than 1 kHz (Figs. 6(a)–6(c)); this result is in close agreement with theoretical predictions. We also predict maximum displacements across the full range of ω and $\bar{V}$ tested (Fig. 6(c)). These results are the first demonstration of an *in situ* actuator that can achieve displacements of $O(10^{-5})$ m at kHz frequencies, while immersed in water. The mathematical model for low-Q physics and design optimization algorithm are sufficiently general such that we can predict and optimize performance for diverse applications ranging from kHz frequency mechanical force probes to local acoustic generators.

ACKNOWLEDGMENTS

This work was supported in part by National Science Foundation CAREER Award No. DBI-1254185, a UCLA Jonsson Comprehensive Cancer Center Seed Grant, as well as UCLA and University of Notre Dame capitalization funds.

APPENDIX: MATRIX CONSTRUCTIONS

Equation (4c) utilizes four $2N+1 \times 2N+1$ matrices that act on the harmonic basis function $T(\tau)$. Matrices $\mathbf{\Delta}$, $\mathbf{C}_1$, and $\mathbf{C}_2$ perform a simple change of basis in the coefficients in X and are thus presented without details. Matrix $\mathbf{\Gamma}(X)$ is complex and, thus, we provide basic details

$$\mathbf{\Delta} = \begin{bmatrix} 0 & 0 & 0 & 0 & 0 & \ldots & 0 & 0 \\ 0 & 0 & 1 & 0 & 0 & \ldots & 0 & 0 \\ 0 & -1 & 0 & 0 & 0 & \ldots & 0 & 0 \\ 0 & 0 & 0 & 0 & 2 & \ldots & 0 & 0 \\ 0 & 0 & 0 & -2 & 0 & \ldots & 0 & 0 \\ \vdots & \vdots & \vdots & \vdots & \vdots & \ddots & \vdots & \vdots \\ 0 & 0 & 0 & 0 & 0 & \ldots & 0 & N \\ 0 & 0 & 0 & 0 & 0 & \ldots & -N & 0 \end{bmatrix},$$

$$\mathbf{C}_1 = \begin{bmatrix} 0 & \frac{1}{2} & 0 & 0 & 0 & \ldots & 0 & 0 & 0 \\ 1 & 0 & 0 & \frac{1}{2} & 0 & \ldots & 0 & 0 & 0 \\ 0 & 0 & 0 & 0 & \frac{1}{2} & \ldots & 0 & 0 & 0 \\ 0 & \frac{1}{2} & 0 & 0 & 0 & \ldots & 0 & 0 & 0 \\ 0 & 0 & \frac{1}{2} & 0 & 0 & \ldots & 0 & 0 & 0 \\ \vdots & \vdots & \vdots & \vdots & \vdots & \ddots & \vdots & \vdots & \vdots \\ 0 & 0 & 0 & 0 & 0 & \ldots & 0 & 0 & \frac{1}{2} \\ 0 & 0 & 0 & 0 & 0 & \ldots & 0 & 0 & 0 \\ 0 & 0 & 0 & 0 & 0 & \ldots & \frac{1}{2} & 0 & 0 \end{bmatrix},$$

$$\mathbf{C}_2 = 2\mathbf{C}_1^2 - \mathbf{I},$$

where $\mathbf{I}$ is the identity matrix. $\mathbf{\Gamma}(X)$ is a complicated matrix that is best expressed by the change in coefficients on the harmonic basis for the equation $x^2(\tau) \approx T(\tau)F$. $F(X) \in \mathbb{R}^{2N+1\times 1}$ is a vector of nonlinear functions of the unknown coefficients in X (Eq. (6))

$$F_0 = A_0^2 + \frac{1}{2}\sum_{i=1}^{N}\left(A_i^2 + B_i^2\right),$$

and

$$\begin{aligned} F_{2j-1} &= A_0 A_j + \sum_{i=0}^{N} A_i A_{i+j} + \sum_{i=1}^{N} B_i B_{i+j} \\ &\quad + \frac{1}{2}\sum_{i=1}^{j-1}\left(A_i A_{j-i} - B_i B_{j-i}\right), \\ F_{2j} &= A_0 B_j + \sum_{i=0}^{N} A_i B_{i+j} - \sum_{i=1}^{N} A_{i+j} B_i \\ &\quad + \frac{1}{2}\sum_{i=1}^{j-1}\left(A_i B_{j-i} + A_{j-i} B_i\right) \end{aligned} \tag{A1}$$

for $j = 1, 2, \ldots, N$. Each A_i or B_i term in Eq. (A1) must exist in the coefficient space X. Terms exceeding this space are assumed to be small and approximately equal to the coefficient on the highest order harmonic: $A_i = A_N$ or $B_i = B_N$ for $i > N$; $\sum_{\alpha}^{\beta}(\cdot) = 0$ for $\alpha > \beta$. $x^2(\tau)$ is rewritten as $x^2(\tau) \approx T(\tau)\Gamma(X)X$, where $\Gamma(X) = \frac{1}{2}\frac{\partial F}{\partial X}$.

[1]M. Meier, R. Sit, and S. R. Quake, Proc. Natl. Acad. Sci. U.S.A. **110**, 477 (2013).
[2]D. Qi, D. J. Hoelzle, and A. C. Rowat, Eur. Phys. J. Spec. Top. **204**, 85 (2012).
[3]M. A. Unger, H.-P. Chou, T. Thorsen, A. Scherer, and S. R. Quake, Science **288**, 113 (2000).
[4]A. R. Abate, J. J. Agresti, and D. A. Weitz, Appl. Phys. Lett. **96**, 203509 (2010).
[5]S. Yazdi and A. M. Ardekani, Biomicrofluidics **6**, 044114 (2012).
[6]J. Chae, H. Kulah, and K. Najafi, J. Micromech. Microeng. **15**, 336 (2005).
[7]J. Dong and P. M. Ferreira, J. Microelectromech. Syst. **18**, 641 (2009).
[8]J. S. Jeong, J. W. Lee, C. Y. Lee, S. Y. Teh, A. Lee, and K. K. Shung, Biomed. Microdevices **13**, 779 (2011).
[9]J. H. Seo and O. Brand, J. Microelectromech. Syst. **17**, 483 (2008).
[10]J. E. Sader, J. Appl. Phys. **84**, 64 (1998).
[11]R. Lifshitz and M. Cross, *Review of Nonlinear Dynamics and Complexity*, Chapter: Nonlinear Dynamics of Nanomechanical and Micromechanical Resonators (Wiley, New York, 2008).
[12]V. Mukundan and B. L. Pruitt, J. Micromech. Microeng. **18**, 405 (2009).
[13]Y. Sun, D. Piyabongkarn, A. Sezen, B. Nelson, and R. Rajamani, Sens. Actuators, A **102**, 49 (2002).
[14]J. F. Rhoads, S. W. Shaw, and K. L. Turner, J. Dyn. Syst. Meas. Control **132**, 034001 (2010).
[15]D. Finkel, *DIRECT Optimization Algorithm*, see http://www4.ncsu.edu/ctk/Finkel_Direct/Direct.m, 2004.
[16]R. M. Lewis, V. Torczon, and M. W. Trosset, J. Comput. Appl. Math. **124**, 191 (2000).
[17]L. K. Forbes, J. Aust. Math. Soc., Ser. B **29**, 21 (1987).
[18]V. Méndez, C. Sans, D. Campos, and I. Llopis, Phys. Rev. E **81**, 066201 (2010).
[19]M. Guskov, J.-J. Sinou, and F. Thouverez, in *IMAC: Conference and Exposition on Structural Dynamics* (St. Louis, MO, USA, 2006).
[20]B. Legrand, A.-S. Rollier, D. Collard, and L. Buchaillot, Appl. Phys. Lett. **88**, 034105 (2006).